

## Highlights

### **Piecewise Constant Strain Kinematic Model of Externally Loaded Concentric Tube Robots**

Mahdi Pourafzal, Ali Talebi, Kanty Rabenorosoa

- Presenting a kinematic model of CTRs based on piecewise constant strain assumption
- Using energy minimization to describe the torsional compliant structure of tubes
- Satisfying distal torsion constraint by torsional Jacobian and Lyapunov method
- Developing a fast and numerically stable solution not dependent on sensing data
- Model validation in both point and distributed external force conditions

# Piecewise Constant Strain Kinematic Model of Externally Loaded Concentric Tube Robots

Mahdi Pourafzal<sup>a</sup>, Ali Talebi<sup>a,\*</sup> and Kanty Rabenorosoa<sup>b</sup>

<sup>a</sup>Department of Electrical Engineering, Amirkabir University of Technology, Tehran 15914, Iran

<sup>b</sup>FEMTO-ST Institute, Univ. Bourgogne Franche-Comte, CNRS, F-25000 Besançon, France

## ARTICLE INFO

### Keywords:

Concentric tube robot  
Helical kinematics  
External loading  
Torsional Jacobian

## ABSTRACT

This paper presents a piecewise constant strain kinematic model for concentric tube robots (CTR) in externally loaded conditions. It discretizes the pre-curved tubes comprising the robot into a finite number of pieces and involves external effects as a set of wrench vectors exerted along the robot backbone. Constant strain lets us describe the pieces with helices in which shear deformation and elongation are neglected. The resulting piecewise helix is the simplest curve that can catch the torsion of tubes that play a crucial role in kinematic behavior. This approximation transforms the conventional boundary value problem (BVP) of CTRs models into a set of nonlinear equations that drastically decreases the model resolution time. The present method uses a Lyapunov function and torsional Jacobian to ensure the distal torsion constraint consistently and, as a result, the solution's convergence. The paper's primary purpose is to present a fast, numerically stable, and relatively accurate kinematic model not reliant on measurement data. Experimental results on a two-tube prototype and provided for different tip loading conditions reveal maintaining a balance between adequate accuracy and reasonable running time, about 7 ms for five pieces per section, for real-time applications in the presence of external load.

## 1. Introduction


Concentric tube robots (CTRs), as an emerging surgical platform [5] have attracted widespread interest in the past decade. Multiple, pre-curved, elastic tubes assembled in a telescopic manner form these thin continuum robots. The tubes, typically made from Nitinol (NiTi), can rotate and translate independently and create diverse shapes of the robot due to their elastic interaction. The intrinsic flexibility and small dimension of CTRs are vital enablers to extend the use of this kind of continuum robots into delicate environments such as the human body, where safe interactions with the anatomy are imperative [2, 1]. Besides, the structural compliance serving infinite degrees of freedom enhances these continuous shape robots' dexterity to perform complex tasks in confined space, particularly in minimally invasive surgery [8, 4]. However, since CTRs rely on the equilibrium of force and moment to establish their ultimate shape, their modeling is more complicated than conventional rigid-link manipulators. They call for fast and accurate enough kinematics to obtain reliable motion control in an unknown environment, which is vital for their further expansion. Piecewise constant curvature (PCC) is the most widely used kinematic model for the different kinds of continuum robots, including CTRs, in which segments are considered circular arcs [42, 6]. This simplified kinematic model defines an intermediate called configuration space to relate actuator and task spaces. Accordingly, the kinematics is decomposed into two mappings, one from the actuator to configuration space and the other from the configuration to task space. Despite being handy, the simplifying constant curvature assumption

is not always valid for CTRs. In reality, the curvature may be variable along their length for a variety of reasons such as fabrication errors, unmodeled phenomena (such as frictions [23] and torsional deformation [9]), and external load. Furthermore, recently, there has also been an increasing interest in designing non-circular shape manipulators [14, 28, 12].

Characterizing the kinematics of continuum robots with variable curvature has been the subject of a large part of literature in the first years of this decade [36, 34]. They departed from the constant curvature assumption and investigated the kinematic behavior of continuum robots in the presence of external load and by taking into account more details like friction [23] and clearance [19] on the subject of CTRs kinematics. Consequently, significant infinite DoF models using Cosserat rod (and its particular case Kirchhoff rod theory) [34] and energy consideration [37] have been developed to describe the kinematic behavior of CTR. The resultant equilibrium equations governing elastic deformation form a boundary value problem (BVP) with split boundary conditions. The shooting method has been the most widely used approach to solve CTR models numerically, but no consensus has emerged in the best way [15]. In [22], different CTR models based on the Cosserat rod theory are compared in computational efficiency. However, the results show that the models derived cannot be acceptable for real-time applications. Different approaches have been developed recently to decrease computation time, giving a reasonably accurate shape of externally loaded continuum robots.

Data-driven methods have been highlighted in the last five years of research to present kinematic models with a lower computational cost. They exploited the truncated Fourier series [20], modal approach [7], locally weighted projection regression [11], and neural networks [21, 47, 16, 13, 17] to bring out a kinematic model executable in real-

\*Corresponding author

 m.pourafzal@aut.ac.ir (M. Pourafzal); alit@aut.ac.ir (A. Talebi); kanty.rabenorosoa@femto-st.fr (K. Rabenorosoa)

time applications [20]. Regression methods and neural networks, because of their universal approximation property, are an effective means to put forward alternative curves for simple constant curvature ones in the configuration space to capture more deformation modes.

In parallel with developing data-driven approaches, much attention in the past few years has been devoted to reducing the theoretically possible redundancy of a soft or continuum manipulator to a few degrees of freedom by discretizing it along its backbone. In [41], a piecewise kinematics of CTRs proposed in which tubes are assumed torsionally compliant only in their transmission sections. Generally, employing constant-curvature subsegments has been a conventional method for discretizing torsionally stiff continuum robots [24, 33, 32]. Recent works in soft robots modeling [29], [30] has been focused on developing a discrete model by discretizing continuous Cosserat based approaches that take into account shear and torsional deformations. This kind of model, called piecewise constant strain (PCS), is in line with the PCC idea and conceptually pursues reducing the dimension of the configuration space by assuming the deformation is piece-wisely constant along the robot length. Consequently, a finite set of strain vectors describes the soft manipulator and plays the same role as the joint vector for traditional robotics.

Reducing the computation cost of models-based kinematics of CTRs is possible by decreasing the number of iteration cycles or the time taken to complete one of them. Sensing the unknown proximal boundary conditions with torque sensors at the tube bases eliminates the need for multiple iteration cycles and concerns about kinematics convergence [45, 44]. However, employing torque sensors, despite offering a rapid and stable solution, complicates actuation mechanism design, and also, the found solution does not necessarily fulfill distal conditions. Simplifications such as piecewise linearization is an effective way to enhance the speed of the solution [15] by decreasing the average time of iterations.

The importance of considering torsion effects in CTR's kinematic models was reflected in [43], while the shear strain is often considered negligible. Due to this simplifying assumption, the pieces of a PCS model can be relaxed into helices, and piecewise helix curves can describe tube shapes. A curve is called a piecewise helix if it comprises a finite number of segments, each of them is a helix. Furthermore, a point where two consecutive segments meet will be called a corner of a piecewise helix [39]. By extending the robot-independent map of the PCC model, a map between helical configuration and task space was presented in [18]. Torsions of tubes can be sensed online by helically-wrapped FBG in [46]. However, unfortunately, it decreases measurable curvature range and requires to engrave slots on the surface of tubes that seems impractical for more narrow tubes.

Previous studies on model-based kinematic approaches of CTRs have failed to achieve a fast and numerically stable solution not dependent on measurement data (Table 1). To the best of our knowledge, a PCS kinematic model for CTRs with concentrated force and moment has never been

presented. This proposed method enables to speed up the computation of forward kinematic of CTRs in the presence of external loads. The discretized structure allows us to obtain the torsional Jacobian of tubes with a less computational cost. It transforms the BVP resolution into a closed-loop switched system under a dwell time constraint, where multiple Lyapunov functions prove the stability of subsystems. A lasting shape of CTR must satisfy two basic constraints: 1) the potential elastic energy stored along a tube length should be minimum, and 2) the last piece of each tube should meet the distal torsional condition imposed by the external tip moment. The remainder of the paper is organized as follows. The second section presents a fast and stable solution of CTR kinematics by approximating the shapes of the tubes comprising a CTR. The suggested kinematics accuracy is demonstrated through simulation by comparing it with a Cosserat exact model and experimental validation with a two-tube prototype proposed in section III. The conclusion appears in the final section.

## 2. Helical Kinematics of Concentric tube Robots

In this section, we put forward a simplified kinematic model to facilitate real-time applications. Indeed, we exploit the idea of piecewise constant strain [29], which has been extended to Kirchhoff and other beams [31], to depict the tube shapes of a CTR. Before discussing the details, we need to make some assumptions and definitions.

### 2.1. Assumptions

Throughout the paper, we make a set of simplifying assumptions significantly decrease computation cost and help to develop an efficient kinematic model A1) Tubes are supposed to bend or twist elastically, but not undergo cross-section shear and axial elongation. It is the Kirchhoff assumption generally regarded as reasonable assumptions for long thin rods like the tubes [37]. A2) The stiffness of tubes in bending and torsion is assumed to be linear elastic. A3) External loading is exclusive to a set of point wrenches exerted at the backbone. It is also noteworthy that some details such as clearance and friction among the tubes are assumed quite negligible. A4) Tubes are divided into pieces with the constant strain (helices) over which the curvature and torsion of the tubes are considered constant.

Mathematically, under the Kirchhoff assumption, a tube's centerline curve can fully describe its shape in a deformed and undeformed state, as shown in Fig 1. This curve can be considered as a regular curve, with nonzero curvature at each point. The following theorem shows that a curve, consisting of a series of helical arcs, can reconstruct the continuous shape of tube centerline  $\Gamma$  and remain inside a tubular region surrounding it.

**Theorem 1** ([39]). *Let  $\Gamma : r(s), 0 \leq s \leq L$  be a regular curve whose curvature  $\kappa(s)$  is nowhere zero. Then for any given  $\epsilon > 0$  there exist a piecewise circular helix  $\bar{\Gamma} : \bar{r}(s)$ ,*

**Table 1**

Comparing previous kinematic models developed of CTRs in terms of computation time, accuracy, need of precomputation, dependence to measured data and easiness to derive robot control.

Method	Computation time	Model accuracy <sup>a</sup>	Disadvantage	Easiness to derive robot control
Piecewise constant curvature [38]	<1ms	Highly depends on external load	External load effects are not included	High
Cosserat rod [34]	15.2 s - 51.2 s (see [22])	1.5%-3%	High computation cost and lack of convergence guarantee	Low
Derivative Propagation [35]	40 ms	Not reported	lack of convergence guarantee	Medium
Truncated Fourier series[10, 20]	<1ms	1.1% -3.1%	Need for precomputation	High
Piecewise linearization and Proximal torque sensor [45, 44]	<1ms	1% -3%	Dependence to measured data	High
Neural network [17]	Not reported	1%	Need for precomputation	High

a. The tip errors divide by the length of robot

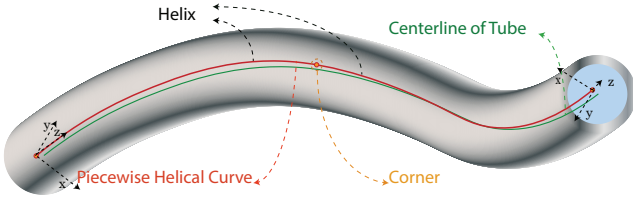


**Figure 1:** Deformed elastic tube whose center-line curve ( $\Gamma$ ) is approximated by piecewise curve ( $\bar{\Gamma}$ ) composed from a set of serially connected helices, each two adjacent of which meet at the corners.

such that

$$|r(s) - \bar{r}(s)| < \varepsilon$$

*Proof.* The proof is given in [39].  $\square$

In the above theorem,  $\varepsilon$  has been proved to be inversely related to the number of pieces.

## 2.2. Helical Approximation of a CTR

Let  $i = 1 \dots n$  denotes the number of the not fully overlapped tubes of a CTR numbered from the innermost to the outermost. Accordingly, the robot length is divided into  $n$  sections indexed from the proximal end to the distal one. We use Bishop frame  $C_B(s)$  to define the reference local coordinates along the CTR length, and Frenet frame  $C_i(s) (i = 1 \dots n)$  to describe the tube curves at an arbitrary arc-length  $s$ . Notice that  $z_B(s)$  and  $z_i(s)$  are tangent to the centerline curve of the robot. Now, suppose a set of distinct points along the backbone, known as corners, on which external point wrenches act.

$$S = \{0 \quad s_1 \quad s_2 \quad \dots \quad L\}, \quad S \subset [0, L] \quad (1)$$

This set can be split into  $n$  subsets denoted by  $S_i (i = 1 \dots n)$ , which contains the corners placed in section  $i$  of the CTR. Moreover, we define subset  $S_e$  as follow

$$S_e(s) = \{s_j \in S | s_j \geq s\} \quad (2)$$

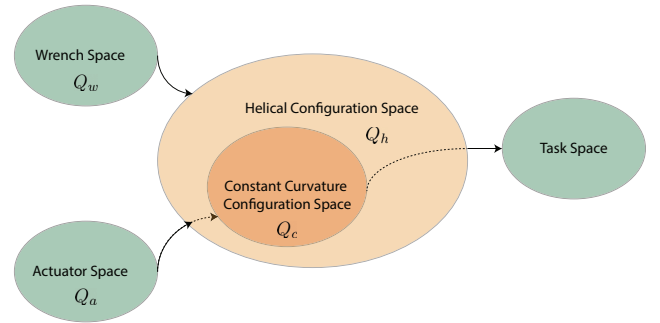


**Figure 2:** The spaces and mappings that define helical kinematics of CTRs. The configuration space of helical kinematics is indeed a broader version of well-known constant curvature configuration space. When a CTR meets the assumption of constant curvature, its configuration is limited to subspace  $Q_c$ .

Moreover, the spatial position of and the wrenches acting on  $s_j \in S$  are denoted as  $p_j$  and  $w_j$ . The definition of spaces in this model structure, as depicted in Fig 2, is almost in line with what is defined in the piecewise constant curvature model [42], but it appends a new space, called wrench space, to import external load. Also, configuration space  $Q_h$ , presented here, is a broader version of constant curvature configuration space  $Q_c$  and includes more complex shapes accessible by a CTR but out of reach by its PCC model. Now, Let  $g : (Q_a, Q_w) \rightarrow SE(3)$  be the helical forward kinematic map of an  $n$ -section CTR, the inputs of which are defined as

$$(q, w) \in (Q_a, Q_w)$$

where  $q = [\alpha_1 \quad \beta_1 \quad \dots \quad \alpha_n \quad \beta_n]$  is a vector in actuator space  $Q_a$ , (in which  $\alpha_i$  and  $-\Delta\beta_i$  denotes rotation at the base and translation of tube  $i$ ) and  $w = \{w_1 \quad w_2 \quad \dots \quad w_{|S|}\}$  is a set of wrench vectors in space  $Q_w$ , each of which is applied at corresponding corner  $s_j \in S$  along the backbone, and is defined as follow

$$w_j = [f_j^T \quad l_j^T]^T, \quad j = 1, \dots, |S| \quad (3)$$

where  $f_j$  and  $l_j$  denote, respectively, force and moment applied on corner  $j$ . If the variables move along a path in  $Q_a$  and  $Q_w$ , the configuration and pose variables of the CTR traverses corresponding ones in helical configuration space  $Q_h$

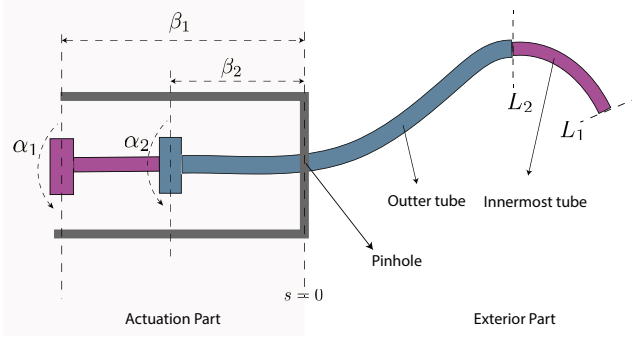


**Figure 3:** Diagram showing actuation and exterior parts of a CTR, where actuation variables  $\alpha_i$  and  $\beta_i$ , respectively, denote the proximal base rotation and translation of the  $i$ th tube.

and, consequently, in task space.

Tubes are actuated independently at the arc-length  $s = -\beta_i$ , where  $\beta_i$  is the transmission length of tube  $i$  followed by the curved exterior part  $L_i$  (see Figure 3).

As is evident from the structure of CTRs, different configurations are the outcome of the equilibrium situation among the elastic pre-curved tubes concentrated and composing the robot. The centerline curves of the deformed tubes are equal and can be nominated by  $r(s)$ . The deformed shape of a tube obeys the elastic interplay in  $x$  and  $y$  axes, while the torsional deformation of a tube occurs independently about the  $z$ -axis. Consequently, they experience a common curvature and different torsions. Therefore, as illustrated in Figure 4, at any arc length  $s$ , reference coordinate frame  $C_B(s)$  can be transformed to tube frame  $C_i(s)$  by a rotation with twist angle  $\theta_i(s)$  about  $z_B$ . The change rate of coordinate frame  $C_i(s)$  to arc length  $s$  or, in other words, the strain vector experienced by  $i$ th deformed tube at cross-section  $s$ , in reference frame  $C_B(s)$  is expressed as

$$\zeta_i(s) = [e_3^T \quad u_i(s)^T]^T \quad (4)$$

where, given the assumption A1,  $e_3 = [0 \quad 0 \quad 1]^T$  and angular strains is of the following form

$$u_i(s) = [-\kappa(s) \sin \phi(s) \quad \kappa(s) \cos \phi(s) \quad \tau_i(s)]^T \quad (5)$$

in which  $\kappa(s)$  and  $\phi(s)$  are the curvature and bending angle of the CTR, and  $\tau_i$  is the torsion of tube  $i$ .

To compute the deformations, we need the equations that relate internal moment to external wrench, then a constitutive model that relates cross-section angular strain  $u_i(s)$  to bending moment. Finally, we can make the shape of CTR by obtaining the angular strains of tubes.

The two first components of the internal moment vector which the material of  $[s, l]$  exerts on that of  $[0, s)$  are

$$\begin{bmatrix} m_x(s) \\ m_y(s) \end{bmatrix} = R_B^T(s) \sum_{\{k|s_k \in S_e(s)\}} ((\hat{p}_k - \hat{r}(s))f_k + l_k) \Big|_{x,y} \quad (6)$$

where  $R_B(s)$  is a rotation matrix from base to body frame coordinate. The third component of the internal moment vector of  $i$ th tube is also related to subset  $S_i$  because there is no

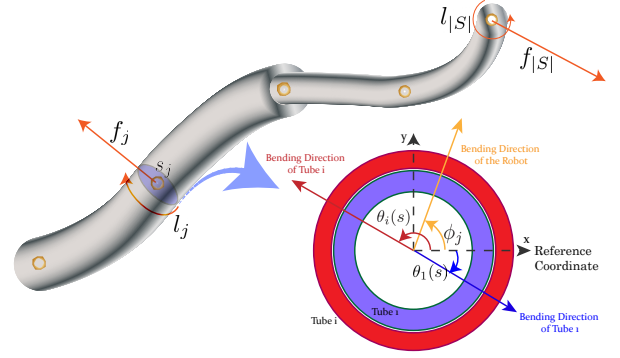


**Figure 4:** The scheme of a CTR on which applied forces are depicted. The yellow spots indicates the element of corner set  $S$  and  $f_{|S_{e^i}|}$  is the force applied to the distal point. The cross section at arc length  $s_j \in S$  is demonstrated where angles  $\theta_1$ ,  $\theta_i$  and  $\phi_j$  express the bending directions of the innermost tube,  $i$ th tube (as a general outer tube) and the CTR in Bishop frame  $C_B(s)$ .

torsional interaction among tubes. So, it is defined as

$$m_{z_i}(s) = e_3^T R_B^T(s) \sum_{\{k|s_k \in S_e(s) \cap S_i\}} ((\hat{p}_k - \hat{r}(s))f_k + l_k) \quad (7)$$

Considering the elastic interaction in  $x$ - $y$  axes, one can define the bending and torsional moment of CTR in terms of tube moments given in (6) and (7).

$$\begin{bmatrix} m_x(s) \\ m_y(s) \end{bmatrix} = \sum_i m_i(s) \Big|_{x,y}, \quad m_{z_i}(s) = m_i(s) \Big|_z \quad (8)$$

The bending moment acting on tube  $i$  makes an elastic deformation from initial strain  $u_i^*(s)$  to new strain  $u_i(s)$ . Given assumption A2, this relation can be described by a linear constitutive model

$$m_i(s) = K_i(u_i(s) - u_i^*(s)) \quad (9)$$

in which  $K_i$  is stiffness matrix (for bending and twisting) defined as

$$K_i = \text{diag}(E_i I_i, E_i I_i, G_i J_i) \quad (10)$$

where  $E_i$  is Young's modulus,  $I_i$  is the area moment of inertia,  $G_i$  is the shear modulus, and  $J_i$  is the polar moment of inertia of  $i$ th tube cross section.

In constitutive equation (9), initial strain  $u_i^*(s)$  denotes the angular strain of tube  $i$  in its unstressed condition and can be given in reference frame  $C_B(s)$  as

$$u_i^*(s) = [-\kappa_i^*(s) \sin \theta_i(s) \quad \kappa_i^*(s) \cos \theta_i(s) \quad \tau_i^*(s)]^T \quad (11)$$

where  $\kappa_i^*(s)$  and  $\tau_i^*(s)$  are pre-curvature and torsion, and  $\theta_i(s)$  denotes the twist angle of  $i$ th tube given as

$$\theta_i(s) = \alpha_i + \int_{-\beta_i}^s (\tau_i)(\xi) d\xi \quad (12)$$

At this point, we go on to find angular strain  $u_i(s)$ . To simplify the calculation, we discretize the backbone into pieces

on which strains are constant. So, each of  $n$  sections, in the exterior part of CTR, is divided into  $m_i$  helical pieces. But in first step, we perform discretization only on curvature parameters as

$$\kappa_j = \kappa(s_j) \quad , \quad \phi_j = \phi(s_j) \quad , \quad \kappa_{i,j}^* = \kappa_i^*(s_j) \quad (13)$$

So, angular strain vectors  $u_i(s)$  and  $u_i^*(s)$  can be turned into the following forms

$$\begin{aligned} \bar{u}_{i,j}(s) &= [-\kappa_j \sin \phi_j \quad \kappa_j \cos \phi_j \quad \tau_i(s)]^T \\ u_{i,j}^*(s) &= [-\kappa_{i,j}^* \sin \theta_{i,j}(s) \quad \kappa_{i,j}^* \cos \theta_{i,j}(s) \quad \tau_i^*(s)] \end{aligned} \quad (14)$$

in which  $j = 1 \dots |S| - 1$ , and  $\kappa_j$ ,  $\phi_j$  and  $\kappa_{i,j}^*$  are constant. Let us focus again on the deformation of a concentric tube and what makes it complicated to model. In such a structure, tubes conform to a common shape determined by elastic interaction while they experience bending and torsional moments and are allowed to twist independently. This twisting behavior is a barrier to being able to predict the shapes of deformed tubes. Torsional deformation can be divided into two categories, the deformation due to external wrenches and the self-deformation that naturally minimizes the elastic energy stored along their lengths. So, we can write torsion  $\tau_i(s)$  as follow

$$\tau_i(s) = \tau_{si}(s) + \tau_{ei}(s) \quad (15)$$

where  $\tau_{ei}(s)$  denotes the torsion caused directly by an external load, and  $\tau_{si}(s)$  is the torsion created to minimize the following energy function.

$$E_{i,j}(s) = \frac{1}{2} (\bar{u}_{i,j}(s) - u_{i,j}^*(s))^T K_i (\bar{u}_{i,j}(s) - u_{i,j}^*(s)) \quad (16)$$

Taking a derivative of (16) with respect to  $s$ , and setting it equal to zero, we get the following condition, for  $s \geq 0$ , that ensures the energy minimization (see Appendix A)

$$\tau_{si}'(s) = \begin{cases} -\frac{\tau_i(s)}{\tilde{\tau}_i(s)} \frac{E_i I_i}{G_i J_i} \kappa_j \kappa_{i,j}^* \sin(\phi_j - \theta_{i,j}(s)) & \|\tilde{\tau}_i(s)\| \geq \delta_\tau \\ + \tau_i'(s) - \tau_{ei}'(s) & \\ \tau_i^*(s) - \tau_{ei}'(s) & \|\tilde{\tau}_i(s)\| < \delta_\tau \end{cases} \quad (17)$$

in which  $\tilde{\tau}_i(s) = \tau_i(s) - \tau_i^*(s)$  and  $\delta_\tau$  is a small positive constant. Finally, by discretizing torsional parameters, we terminate the discretization task.

$$\begin{aligned} \tau_{i,j} &= \tau_i(s_j) \quad , \quad \theta_{i,j} = \theta_i(s_j) \\ \tau_{s(i,j)} &= \tau_{si}(s_j) \quad , \quad \tau_{e(i,j)} = \tau_{ei}(s_j) \end{aligned} \quad (18)$$

Then, (12) and (17) can be converted to

$$\theta_{i,j} = \theta_{i,j-1} + \tau_{i,j-1} L_{i,j} \quad (19)$$

and

$$\tau_{s(i,j+1)} = \begin{cases} -\frac{\tau_{i,j}}{\tilde{\tau}_{i,j}} \frac{E_i I_i}{G_i J_i} \kappa_j \kappa_{i,j}^* L_{i,j} \sin(\phi_j - \theta_{i,j}) & \|\tilde{\tau}_{i,j}\| \geq \delta_\tau \\ + \tau_{s(i,j)} + \Delta \tau_{i,j}^* - \Delta \tau_{e(i,j)} & \\ \tau_{s(i,j)} + \Delta \tau_{i,j}^* - \Delta \tau_{e(i,j)} & \|\tilde{\tau}_{i,j}\| < \delta_\tau \end{cases}$$

(20)

where  $L_{i,j}$  denotes the length of helix  $j$ . Consequently, the constant strain vector of tube  $i$ , for  $s \geq 0$ , can be given as

$$\zeta_{i,j} = [e_3 \quad -\kappa_j \sin \phi_j \quad \kappa_j \cos \phi_j \quad \tau_{i,j}] \quad (21)$$

Note that for  $s < 0$ , the ultimate curvature is considered zero. So, from (17), we find that pre-torsion is the only reason to change torsion in the transmission part.

$$\theta_{i,1} = \alpha_i + \int_{-\beta_i}^0 (\tau_{i,1} + \tau^*(\xi)) d\xi \quad (22)$$

For now, we assume proximal torsion  $\tau_{i,1}$  and the position of corners in (6) and (7) are available and focus on completing the approximation of CTR by obtaining  $\phi_j$ ,  $\kappa_j$  and  $\tau_{e(i,j)}$ . So, by using the constructive law (9), angular strain vectors (5) and (11), and the discretized parameters given in (13) and (18), we can obtain curvature  $\kappa_j$  and bending angle  $\phi_j$  as

$$\begin{aligned} \begin{bmatrix} \kappa_{x_j} \\ \kappa_{y_j} \end{bmatrix} &= K^{-1} \Big|_{x,y} \left( \sum_{i=1}^{n_j} E_i I_i \kappa_i^* \begin{bmatrix} \sin \theta_{i,j} \\ \cos \theta_{i,j} \end{bmatrix} + \begin{bmatrix} -m_x(s_j) \\ m_y(s_j) \end{bmatrix} \right) \\ \kappa_j &= \sqrt{\kappa_{x_j}^2 + \kappa_{y_j}^2} \quad , \quad \phi_j = \tan^{-1}(\kappa_{x_j}/\kappa_{y_j}) \end{aligned} \quad (23)$$

where  $n_j$  is the number of the tubes overlapping at piece  $j$ . Also, we can get torsion  $\tau_{e(i,j)}$  as

$$\tau_{e(i,j)} = \frac{m_z(s_j)}{G_i J_i} \quad (24)$$

Knowing that  $\tau_{i,j} = \tau_{s(i,j)} + \tau_{e(i,j)}$ , strain vector  $\zeta_{i,j}$  is determined. For drawing the torsion-less centerline of the CTR, we can use constant strain vector  $\zeta_j$  as

$$\zeta_j = [e_3^T - \kappa_j \sin \phi_j \quad \kappa_j \cos \phi_j \quad 0]^T \quad (25)$$

Consequently, helical forward kinematics map  $g_j$  determining position and orientation of the centerline at corner  $j$  can be given by the product of exponential formula [26] as

$$g_j = \begin{cases} \prod_{k=1}^{j-1} e^{\zeta_k L_k} & j = 2, \dots, |S| \\ I_4 & j = 1 \end{cases} \quad (26)$$

### 2.3. Closed Internal Loop

As can be seen in the previous section, we can obtain torsion  $\tau_{i,j}$  and the position of corner  $s_j$  by (26) if proximal torsion  $\tau_{i,1}$ , ( $i = 1 \dots n$ ) and position  $p_k$ , ( $k > j$ ) are known. Referring to (7), (9), and angular strains (5) and (11), one can find that the distal torsion of a CTR is constrained and determined by the external moment applied on the distal point. This characteristic makes the distal boundary condition. So, we must find the proximal torsion which satisfied the distal boundary condition specified by tip external moment.

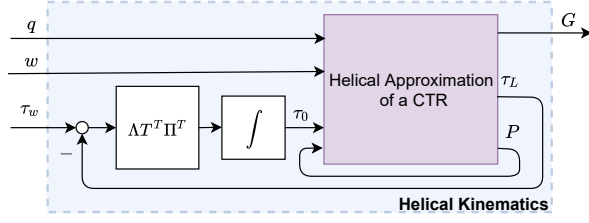


**Figure 5:** Block diagram of the helical kinematic model proposed for CTRs in which  $w$ ,  $q$  are the set of external point wrench and actuator vectors. Output  $P$  contains the position vectors of point-set  $S$  feeded back into the input, and  $G$  is a set of transformation matrices involving all corner nodes' positions and orientations. Distal torsion constraint  $\tau_w$  is the set value for the internal torsional feedback.

Conventional continuous kinematics proposed for CTRs often use shooting methods to solve the split boundary value problem. They find a nominal solution curve consistent with the boundary condition at one end and iteratively update it to satisfy the other end condition. Such a procedure depends on the Jacobian matrix's behavior associated with the differential system under consideration (refer to [25]).

Here, thanks to the solution curve's discretization, we can quickly calculate the Jacobian matrix in each iteration. Using internal feedback, we can offer a fast estimation of proximal torsion and ensure convergence. Now, let us go back to the helical approximation explained in the previous section. External wrenches and actuators are the known inputs, and proximal torsions and the position of corners are the unknown inputs necessary to draw the shape of CTR. Moreover, distal torsion and the position of corners can be considered as outputs. So, the helical approximation can be summarized in the following functions

$$\tau_L = \chi(q, w, P, \tau_0) \quad , \quad P = \xi(q, w, P, \tau_0) \quad (27)$$

where  $P = \{p_1 \ p_2 \ \dots \ p_{|S|}\}$  denotes the position of corners and  $\tau_0 = [\tau_{1,1} \ \tau_{2,1} \ \dots \ \tau_{n,1}]^T$  is proximal torsion vector. Moreover, output  $\tau_L$  in (27) is a vector containing distal torsions.

$$\tau_L = [\tau_{1,|S_1|} \ \tau_{2,|S_1 \cup S_2|} \ \dots \ \tau_{n,|S_1 \cup \dots \cup S_n|}]^T \quad (28)$$

The search for a proximal torsion (input) satisfying the distal torsion (output) condition can be interpreted as internal feedback. In this sense, the position of corners in the output is fed directly back into the input (5), and distal torsion constraint imposed by the external wrenches can be seen as a desired value for output  $\tau_L$  defined by

$$\tau_w = [\tau_{w1,|S_1|} \ \tau_{w2,|S_1 \cup S_2|} \ \dots \ \tau_{wn,|S_1 \cup \dots \cup S_n|}]^T \quad (29)$$

where  $\tau_{wi,|S_1 \cup \dots \cup S_i|}$  is the torsion we expect from the applied moment at the endpoint of tube  $i$ . Since the first two inputs in (27) are known and constant in static conditions, we can use the following theorem to determine the ultimate shape of the CTR.

**Theorem 2.** Let proximal torsion vector  $\tau_0$  is updated by

$$\dot{\tau}_0 = -\Lambda T_{\sigma(t)}^T \Pi^T (\tau_L - \tau_w)$$

where  $T_{\sigma(t)} = \frac{\partial \chi}{\partial \tau_0} + \frac{\partial \chi}{\partial P} (I - \frac{\partial \xi}{\partial P})^{-1} \frac{\partial \xi}{\partial \tau_0}$  and  $(I - \frac{\partial \xi}{\partial P})$  is invertible,  $\Pi$  and  $\Lambda$  are positive definite and diagonal position definite matrices. Then helical kinematic model converges to the desired distal torsion condition.

*Proof.* Let  $V = (\tau_L - \tau_w)^T \Pi (\tau_L - \tau_w)$  be a Lyapunov function for (27), we form the differential as  $\dot{V} = (\tau_L - \tau_w)^T \Pi \dot{\tau}_L$ . So, to prove satisfying the desired distal condition, we must have

$$\dot{V} < -(\tau_L - \tau_w)^T Q (\tau_L - \tau_w) \quad , \quad Q > 0 \quad (30)$$

By differentiating from (27), recalling that  $q$  and  $w$  are constant, we have

$$d\tau_L = \frac{\partial \chi}{\partial \tau_0} d\tau_0 + \frac{\partial \chi}{\partial P} dP \quad (31)$$

and

$$dP = \frac{\partial \xi}{\partial \tau_0} d\tau_0 + \frac{\partial \xi}{\partial P} dP \quad (32)$$

we can rewrite it as

$$dP = (I - \frac{\partial \xi}{\partial P})^{-1} \frac{\partial \xi}{\partial \tau_0} d\tau_0 \quad (33)$$

From (31) and (33), torsional Jacobian  $T_{\sigma(t)}$  is obtained

$$T_{\sigma(t)} = \frac{\partial \tau_L}{\partial \tau_0} = \frac{\partial \chi}{\partial \tau_0} + \frac{\partial \chi}{\partial P} (I - \frac{\partial \xi}{\partial P})^{-1} \frac{\partial \xi}{\partial \tau_0} \quad (34)$$

Note that we consider  $N$  modes of operation, each of which involving a set of close configurations and  $\sigma(t) : t \rightarrow \{1 \ \dots \ N\}$  denotes the switching signal that ascertains the linear subsystem (torsional Jacobian) associated with the activated mode. Matrix  $(I - \frac{\partial \xi}{\partial P})$  is invertible as long as corner position  $P \in S$  is affected by proximal torsion vector  $\tau_0$ . So, proximal and distal torsion vectors are updated by

$$\dot{\tau}_0 = -\Lambda T_{\sigma(t)}^T \Pi^T (\tau_L - \tau_w), \quad \dot{\tau}_L = T_{\sigma(t)} \dot{\tau}_0 \quad (35)$$

where  $\Lambda$  is a diagonal position definite matrix. Substituting  $\dot{\tau}_L$  and  $\dot{\tau}_0$  into  $\dot{V}$  yields

$$\dot{V} = -(\tau_L^T - \tau_w) \Pi T_{\sigma(t)} \Lambda T_{\sigma(t)}^T \Pi^T (\tau_L^T - \tau_w) \quad (36)$$

Considering  $Q = \Pi T_{\sigma(t)} \Lambda T_{\sigma(t)}^T \Pi^T$ , condition (30) is satisfied. Switching signal  $\sigma(t)$  is said to have dwell time  $t_D > 0$  if  $t_{k+1} - t_k \geq t_D$ , where  $t_k$  and  $t_{k+1}$  are consecutive switching instants. When all individual subsystems are asymptotically stable, there exists a dwell-time  $t_D$  that allows the transient effect to dissipate after each switch (see Theorem 3.1 of [27])  $\square$

### 3. Simulation and Experimental Results

To evaluate the precision of the helical kinematics and resolution method developed in section 2, a set of simulations and experimental implementations were carried out for a CTR in various configurations and under different loading conditions.

#### 3.1. Evaluation Criteria

Like in many previous studies on CTRs or other continuum robots, we still use tip error as a metric to evaluate our simulation and experiment results. Nevertheless, we divide it by arc length to normalize the outcomes of the experiments on which the robot has different lengths. So, one can offer the following evaluation criteria

$$J_e = \frac{\|r_{\text{model}}(L_1) - r_{\text{data}}(L_1)\|}{L_1} \quad (37)$$

where  $\|\cdot\|$  denotes Euclidean norm,  $L_1$  is the innermost tube length,  $r_{\text{model}}(L_1)$  is the predicted position and  $r_{\text{data}}(L_1)$  denotes tip position derived from an exact geometric model in simulations and pose sensors in experiments. This error is usually expressed in % of robot length (as proposed in [34, 37]).

#### 3.2. Simulation of CTRs Kinematics

The geometrically exact models based on Cosserat rod theory offer a reasonably accurate kinematic behavior of CTRs but suffer from computational complexity. In [22], through the simulation of two tube CTRs, four different approaches are investigated concerning computational efficiency. One can admit that all these approaches take more than multiple seconds to calculate the ultimate shape. Here, we compare the proposed model with the Cosserat one from [34] in computation time and accuracy.

**Table 2**

Parameters of CTR used during simulation

	Tube 1	Tube 2	Tube 3
Inner Diameter (mm)	0.385	0.55	0.8
Outer Diameter (mm)	0.515	0.76	0.9
Curved Length (mm)	100	50	50
Straight Length (mm)	165	105	85
Young's Modulus (E) (Gpa)	70	70	70
Shear Modulus (G) (Gpa)	26.31	26.31	26.31
Pre-curvature ( $\kappa^*$ ) ( $m^{-1}$ )	6.46	6.2	5

To this aim, we consider a three-tube CTR with parameters listed in table 2 as a framework to address their behavior in the presence of both distributed and concentrated forces. The methods run on an Intel Core i7-7660U CPU running at 2.5GHz. The external moments, in all simulations and experiments, are zero, and the finishing condition is the point at which the norm of distal torsion vector  $\tau_l$  is less than  $0.1N/m^2$ . The switching frequency of torsional Jacobian  $T_{\sigma(t)}$  is considered 25 times smaller than the sample rate. In the simulations, the initial values of  $\tau_0$  and  $P$ , respectively, are a zero vector and the position vectors got

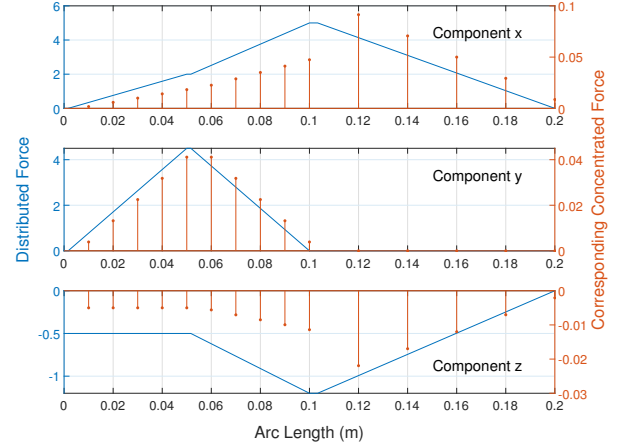


**Figure 6:** Distributed force and its corresponding concentrated force used by helical piecewise model.

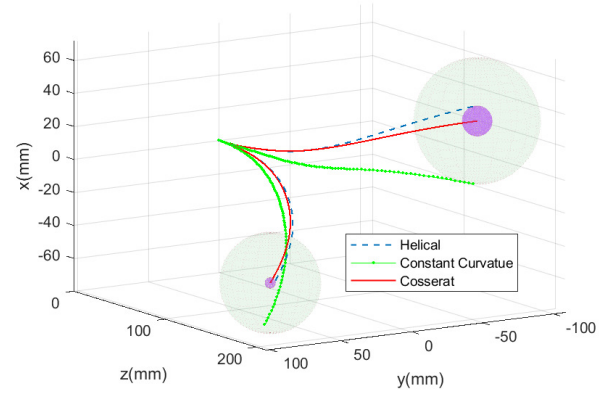


**Figure 7:** The effect of concentrated tip section force on different kinematic models for two selected configurations of 50 tests, two different actuator values have been taken while the same external forces (see Table 3) have been applied to them. The circles radius indicates the tip errors between Cosserat and the two other models.

from the constant curvature model. Figure 7 compares the shapes of two selected configurations derived from the exact geometrical and helical model when concentrated forces listed in Table 3 are applied at the tubes' tip points. Also, the continuous nature of Cosserat models enables us to include distributed forces neglected in discrete ones. So, in helical kinematics, we must consider them as a set of concentrated loads applied on point set  $\mathcal{S}$ . We define concentrated force  $f_j$  as follow to cover the effect of distributed force on piece  $j$

$$f_j = \int_{s_{j-1}}^{s_j} f_d(\sigma) d\sigma \quad (38)$$

The distributed force and corresponding concentrated ones applied to the CTR are indicated in figure 6. Figure 8 shows how a five-piece helical kinematic model can esti-



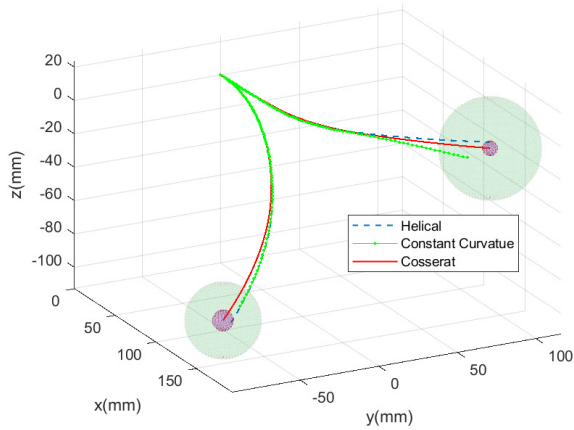


**Figure 8:** The effect of distributed force on different kinematic models for two selected configurations of 50 tests, two different actuator values have been taken while the same external forces (see Fig. 6) have been applied to them. The circles radius indicates the tip errors between Cosserat and the two other models.

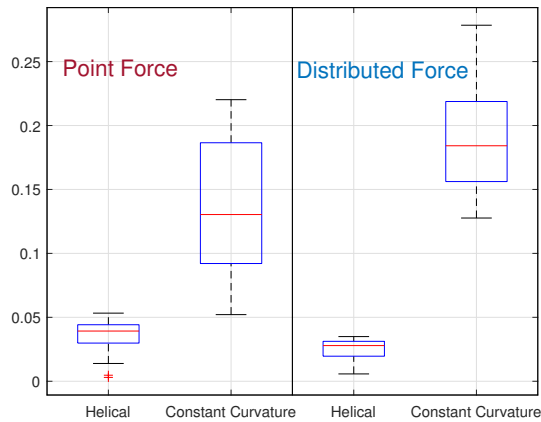


**Figure 9:** The simulation results for 50 tests. The accuracy of helical (10 pieces per section) and constant curvature kinematics is demonstrated by comparing their tip positions with those derived from the exact geometric kinematics.

**Table 3**

The condition of loading in the point force case

Point Force	$F_1 = \begin{pmatrix} 0 \\ 0 \\ -0.1 \end{pmatrix}$	$F_2 = \begin{pmatrix} 0 \\ 0.1 \\ 0 \end{pmatrix}$	$F_3 = \begin{pmatrix} -0.2 \\ 0 \\ 0 \end{pmatrix}$
Application Point	The tip of tube 1, $s = L_1$	The tip of tube 2, $s = L_2$	The tip of tube 3, $s = L_3$

mate the exact shape created by the exact model [34]. We tested 50 different configurations of the CTR while the concentrated and distributed forces were acting on it. Comparing the computation time of these approaches barely reveals that discretizing decreases the computation time. It reduces the average computation time from 72.6s to 11ms for ap-

**Table 4**

Comparison of computation time of kinematic models over 50 configuration tests through simulation, in two different loading conditions depicted in Fig6 and Table 3 .

Kinematic models	Average computation time (sec)	
	Distributed force	Point force
Constant curvature	0.0012	0.0012
Helical	0.069	0.0115
Cosserat rod [34]	236.8	72.6

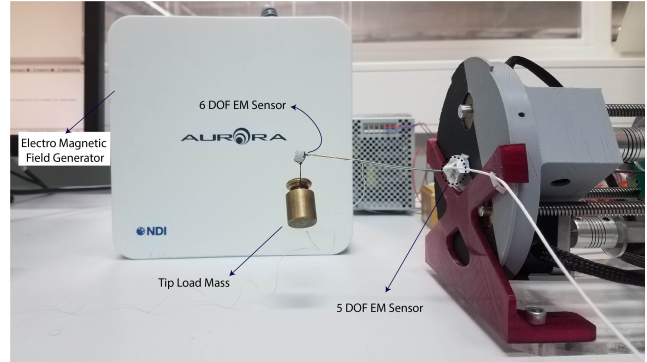


**Figure 10:** Experimental setup consisting of a concentric tube robot, an electromagnetic tracker and two coils mounted at the base and tip of the robot which are used to measure the position.

plied point forces and from 236s to 69ms when a distributed force acts on CTR. Table 4 details the average computation times of the different kinematic models. On the other hand, as highlighted in Fig. 9, the performance criteria (37) of the helical piecewise model reaches comparable performance to that of the Cosserat one [34].

**Table 5**

Physical Quantities For Experimental Tubes

	Tube 1	Tube 2
Inner Diameter (mm)	0.385	0.55
Outer Diameter (mm)	0.515	0.76
Curved Length (mm)	125	65
Straight Length (mm)	165	105
Young's Modulus (E) (Gpa)	70	70
Shear Modulus (J) (Gpa)	26.3	26.3
Pre-curvature ( $\kappa^*$ ) ( $m^{-1}$ )	6.46	6.2

### 3.3. Robot Prototype and Measurement Methods

The experimental platform, as shown in Fig. 10, involves a concentric-tube robot prototype and an Aurora electromagnetic tracking system (EMTS) manufactured by Northern Digital Inc. Two NiTi tubes with physical properties listed in Table 5 comprise the CTR. Each tube has an initial straight length on the actuation unit, followed by a curved section. Tubes are translated and rotated independently, so, to generate the achievable configuration space, one can define the actuator vector of the CTR as  $q_a = [\alpha_1 \ \alpha_2 \ \beta_1 \ \beta_2]$

where  $\alpha_1, \alpha_2 \in [-\pi \ \pi]$ ,  $\beta_1 \in [0.165 \ 0.225]$  and  $\beta_2 \in [0.105 \ 0.135]$ . The outward length of inner and outer tubes in initial configuration are 0.095 and 0.04 respectively. In our experiments, the CTR took four different paths in the actuator space. All start at **common** point  $q_{aI} = [0 \ 0 \ 0.195 \ 0.115]^T$ , but end at different points  $q_{aE} = [\alpha_{1e} \ \alpha_{2e} \ \beta_{1e} \ \beta_{2e}]^T$ . They were sampled at rate  $\delta q_a = [\delta\alpha_1 \ \delta\alpha_2 \ \delta\beta_1 \ \delta\beta_2]^T$ , given in Table 6. The collected data from these different paths made several configurations in which the accuracy of the kinematic model was examined.

As shown in Fig. 10, two 3-D points at the base and endpoint of the robot were determined via the EMT system. Considering **the prototype's dimensions**, it was not difficult to adjust the robot pose and keep its workspace within measurement volume (a cube with edges of about 50cm). Sensors are small coils in which weak currents are induced by the varying electromagnetic field produced by filed generator. As depicted in Fig. 10, we used the Aurora 5DOF Flex Tube at the base because it showed more robustness against the disturbance caused by some metallic components of the actuation unit, and the Aurora Micro 6DOF, the smallest 6DOF sensor offered by NDI, at the endpoint. The system control unit (SCU) sends the position and orientation data to the host computer through a USB connection.

### 3.4. The Kinematic Model Performance

Several probable error sources may affect the performance of the kinematic model and can be divided into two categories. One is unmodeled details, which we call disturbance wrenches, and the other is discretization error.

Clearance and friction are one of the most important details that have been neglected. They occur among the tubes or between the outer tube and the hole drilled in the base plate. The rest includes shear effects, tubes manufacturing errors such as tolerance of pre-curvatures, **pre-torsion**, and length. Besides the **factors mentioned above**, probable uncertainties in the applied force and the sensor observations can also raise the error. **Discretization error usually is more problematic in external loads, where the internal moments caused by them vary along the length of tubes.**

The capability of the proposed model to handle the two mentioned sources of errors is examined experimentally. To draw a complete comparison, we demonstrated the result by box plot which provides statistical properties. Fig. 11 and 12 compare the performance of the proposed model, for the different number of helices, with that of PCC in terms of evaluation criteria (37) and computation time in the absence and presence of external force. In unloaded conditions, the PCC model ensures an acceptable accuracy (see Fig. 11) in a short computation time. However in the presence of a tip point load, as was expected, PCC fails to give an accurate picture of CTRs kinematic behavior (see Fig. 12). Since the pre-curvature of tubes is considered constant, **the curvature of segments must be almost constant in free space conditions**, and disturbance wrenches play the dominant role in

creating the position error. It explains why considering more pieces of helices seems not to affect decreasing errors in the unloaded tests (see Fig. 11), but, in the presence of external loads (see Fig. 12), shows a decrease in the average error. As external forces create internal moments varying along the tubes, this reduction is more prominent with increasing load. As seen in Fig. 11 and 12, the proposed approach produces a trade-off between accuracy and computational cost. Obviously, under heavier load, the kinematic model requires more pieces and inevitably more time to successfully characterize the CTR shape.

In Fig. 13, the accuracy of the kinematics with five helices per section is shown while different weights are applied to the **CTR tip point** and execution time is about 11ms. Also, one can find from Fig. 13 that the model fails to capture the deformation which tip-weight  $M = 50gr$  makes. The effect of tip force on changing the configurations of a CTR is indicated in Fig. 14, where the CTR approximate shapes are shown in free space and loaded with  $M = 15gr$  and  $M = 50gr$  weights, while the actuators are locked. The radius of spheres centered at the distal end of the CTR shows the tip position error.

As expected, the discretization error decreased with increasing the number of pieces, and this reduction is especially noticeable under high loads. The disturbance wrenches is not affected, as a rule, by increasing the degrees of freedom. However, we hope that estimating external wrenches based on position data will reduce the error caused by unmodeled details. The effect of torsion deformation on the kinematics of CTRs is apparent in comparing the performance of PCC with that of the proposed kinematics.

**Table 6**  
Paths of the CTR in the Actuator Space

	Translation (mm)				Rotation (deg)			
	$D_{1e}$	$D_{2e}$	$\delta D_1$	$\delta D_2$	$\alpha_{1E}$	$\alpha_{2E}$	$\delta\alpha_1$	$\delta\alpha_2$
1	165	110	0.2	0.2	180	45	0.5	0.15
2	165	105	0.2	0.1	180	0	0.5	0
3	175	130	0.6	-0.3	90	-90	0.8	-0.8
4	175	130	0.08	-0.1	-270	90	-0.8	0.4

### 3.5. Discussion

The inherent flexibility of thin tubes made of superelastic NiTi alloys allows them to experience complex deformation, including bending and twisting. Shaping tubes into pre-curved configurations and concentrating them creates a small needle-sized tool that can elongate and bend. These enhanced and unique features of CTRs make them ideal for performing delicate surgical maneuvers, although their possible applications can be developed outside medicine in the future [15]. They have been proposed to perform various intracranial procedures where access is difficult and requires penetrating the heart through the vascular system [40]. Moreover, they have been recognized as a reliable instrument for endonasal skull base surgery [3], transoral throat, and other natural orifice surgeries likely to pursue in the future.

The present study suggested a discretized model of CTRs

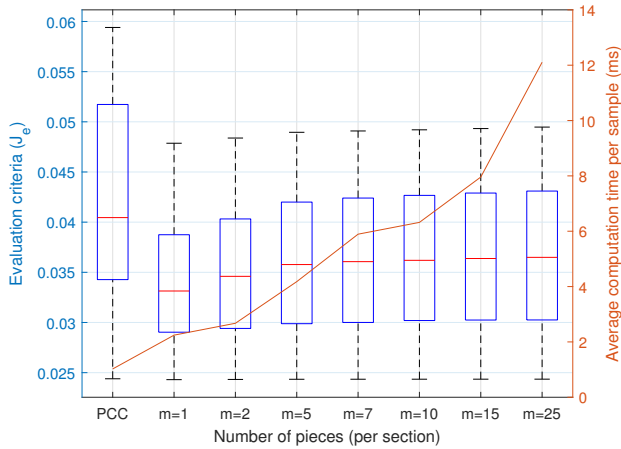


**Figure 11:** Comparison of evaluation criteria  $J_e$  and the computation time of PCC with those of proposed helix-based kinematics for different number of pieces to describe CTR kinematics in free space.

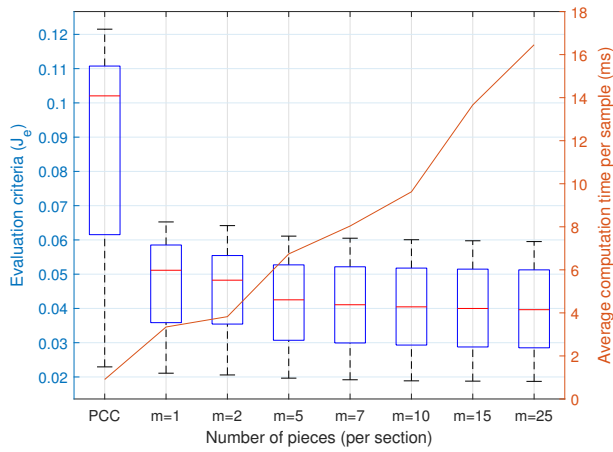


**Figure 12:** Comparison of evaluation criteria  $J_e$  and the computation time of PCC with those of the proposed helix-based kinematics for different number of pieces to describe the kinematics of a CTR on which a 10gr weight is mounted.

by assuming a piecewise constant strain along the tubes. Another novel contribution is that we presented a closed-loop switching system to ensure meeting the distal boundary condition imposed by external moments at the tubes' tip points. In such a scheme, the distal torsions obtained by the constitutive model makes the set value to which torsional output  $\tau_L$  should reach (refer to Fig. 5).

Discretization, by itself, allows us to have less computation in comparison with traditional continuous models. Moreover, the switching frequency is smaller than the control frequency, and since the large portion of the computation is concerned with Jacobian calculation, it significantly reduces the computational cost. Comparing the results of the proposed method with simulations of the Cosserat-based model [34] represents an improvement of computational efficiency in computation time (Table 4). Moreover, compared to the results of simulations, implementations reveal

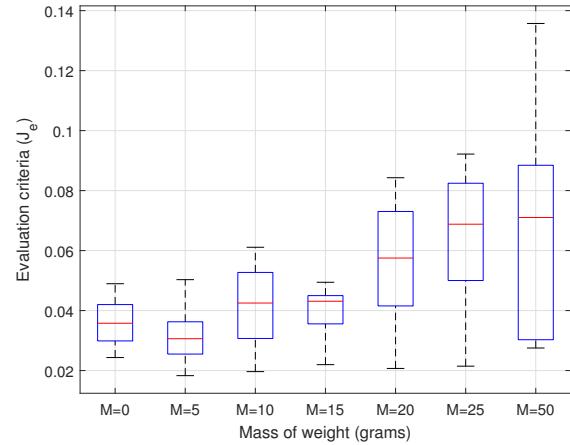


**Figure 13:** The performance of helical kinematics dealing with different tip loads. A weight with mass  $M$  is tied to the tip point of the CTR, and the sections are divided into 5 pieces in all tests.

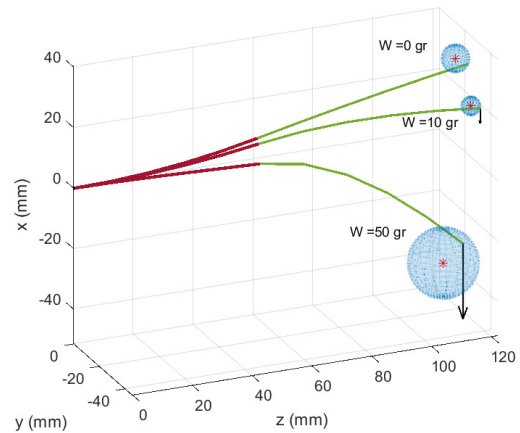


**Figure 14:** Different configurations of a two tube CTR that created by various point forces, while the all actuators are locked. The number of pieces is varied according to the applied forces values. The kinematic behavior of each section is described by two pieces in free space, ( $F = 0$ ), and by five pieces when, 15gr ( $F = 147.15mN$ ) and 50gr ( $F = 490.5mN$ ) weights are hanged at the tip. The radius of the blue sphere indicates the tip error in each case.

a significant decrease in computation time (about 7 ms for an approximation with five pieces per section, see Fig. 12 and 11). An appropriate choice of initial values, the previous step in implementations, accelerates the convergence. However, in all simulations, the initial values come from the PCC model. This work fails to achieve the computation time reported in sensing-based methods [45] (about 1 ms for a three-tube CTR) or data-driven kinematic approaches [47, 16, 13, 17]. However, it is still fast enough to easily be performed at 100 Hz or faster by implementation in C++.

The stability of all individual subsystems is guaranteed by the Lyapunov method. The switching depends on CTR

movement speed, and as long as there are not many sudden changes in environment or actuators, CTRs can be viewed as slowly switched linear systems. So, CTRs can be stable under a dwell time constraint. It means that staying on each mode for a period greater than or equal to  $t_D$  make the system asymptotically stable. Thus, contrary to previous models not dealing with the convergence of the numerical procedure used to solve the boundary value problem of a CTR, the proposed method gives us a characterization of the stability.

Normalized tip position error is the metric to evaluate the accuracy performance of the proposed model. The maximum and average tip position errors between Cosserat [34] and the PCS model are less than 5.5% and 4% of their length in the point force case, and 3% and 2.5% of their length in the distributed force case. It is also worth noting the accuracy of the Cosserat based model [34] is announced about 2% of the length (on average). Some loss of accuracy is the price to pay for obtaining model-based kinematics facilitating the effective control of CTRs. Nevertheless, we hope that external wrench estimation will be beneficial in increasing accuracy, where shape reconstruction techniques [39] based on Fiber Bragg Gratings (FBG) or electromagnetic (EM) sensing help to express the effects of these unmodeled details in terms of disturbing wrenches.

Creating a straightforward analytical framework of CTRs also provides a chance to address other essential aspects of them. We are confident that the proposed model can improve the knowledge about bifurcation, an elastic instability in which the manipulator suddenly releases strain energy and jumps from a critically stable configuration to lower energy, a stable one. Such an abrupt change in configuration, given the CTR's static condition, comes from a sudden change in proximal torsion while the distal condition is unchanged. It probably means the invertibility assumption in Theorem 2 is violated.

## 4. Conclusion and Future Work

This paper proposed a novel kinematic model for CTRs based on piecewise constant strain (PCS) assumption that allows describing tubes by a series of helices. The resulting conformed piecewise helical curves must satisfy two conditions, 1) minimum strain energy along their length 2) the distal torsion constraint imposed by external tip moment. A closed-loop structure presented in which the two mentioned conditions were satisfied, respectively, in forward and feedback directions. We used the torsional Jacobian to linearize CTR at a set of similar configurations and a Lyapunov function to converge it to a valid configuration or a stable state. The stability of the switching system is ensured under dwell-time constraints.

The findings indicate that the computation time is reduced to 7ms for a two-tube CTR while the average tip error is about 4% of the robot length under loading conditions. We hope that the accuracy can be improved through real-time estimating of external loads, using different shape sensing approaches, and including the effect of unmodeled details as an external wrench in PCS structure. Moreover, we think

the resulting analytic framework provides insights for further studies on characterizing of snapping behavior of CTRs.

## Acknowledgement

The work of K. Rabenorosoa was supported by the EIPHI Graduate School (ANR-17- EURE-0002) and ANR  $\mu$ RoCS (ANR-17-CE19-0005).

## A. Minimizing strain energy

Beginning with strain energy (16)

$$E_{i,j}(s) = \frac{1}{2} (\bar{u}_{i,j}(s) - u_{i,j}^*(s))^T K_i (\bar{u}_{i,j}(s) - u_{i,j}^*(s))$$

We differentiate with respect to  $s$  to obtain

$$E'_{i,j}(s) = (\bar{u}_{i,j}(s) - u_{i,j}^*(s))^T K_i (\bar{u}'_{i,j}(s) - u_{i,j}^{*'}(s))$$

From (14), we have

$$\begin{aligned} \bar{u}'_{i,j}(s) &= [0 \quad 0 \quad \tau'_i(s)]^T \\ u_{i,j}^{*'}(s) &= [-\theta'_i(s)\kappa_{i,j}^* \cos \theta_i(s) \quad -\theta'_i(s)\kappa_{i,j}^* \sin \theta_i(s) \quad \tau_i^{*'}(s)] \end{aligned}$$

At the minimum energy, we have

$$\begin{aligned} &(-\kappa_j \sin \phi_j + \kappa_{i,j}^* \sin \theta_i(s)) E_i I_i (\kappa_{i,j}^* \theta_i'(s) \cos \theta_i(s)) \\ &+ (-\kappa_j \cos \phi_j - \kappa_{i,j}^* \cos \theta_i(s)) E_i I_i (\kappa_{i,j}^* \theta_i'(s) \sin \theta_i(s)) \\ &+ (\tau_i(s) - \tau_i^*(s)) G_i J_i (\tau_i'(s) - \tau_i^{*'}(s)) = 0 \end{aligned}$$

From (12), we know  $\theta_i'(s) = \tau_i(s)$ . So, when  $\tau_i(s) \neq \tau_i^*(s)$  the following condition satisfy the minimum energy constraint.

$$\tau_i'(s) = \tau_i^{*'}(s) - \frac{\tau_i(s)}{\tau_i(s) - \tau_i^*(s)} \frac{E_i I_i}{G_i J_i} \kappa_j \kappa_{i,j}^* \sin(\phi_j - \theta_i(s))$$

and when  $\tau_i(s) = \tau_i^*(s)$ , the tube is torsionally relaxed, then the deformed and undeformed configurations of tube  $i$  are in the same plane. So, knowing that  $\phi_j = \theta_i(s)$ , the strain energy is minimum.

## References

- [1] Anor, T., Madsen, J.R., Dupont, P., 2011. Algorithms for design of continuum robots using the concentric tubes approach: A neurosurgical example, in: 2011 IEEE international conference on robotics and automation, IEEE. pp. 667–673.
- [2] Bedell, C., Lock, J., Gosline, A., Dupont, P.E., 2011. Design optimization of concentric tube robots based on task and anatomical constraints, in: 2011 IEEE international conference on robotics and automation, IEEE. pp. 398–403.
- [3] Burgner, J., Rucker, D.C., Gilbert, H.B., Swaney, P.J., Russell, P.T., Weaver, K.D., Webster, R.J., 2013. A telerobotic system for transnasal surgery. IEEE/ASME Transactions on Mechatronics 19, 996–1006.
- [4] Burgner, J., Swaney, P.J., Rucker, D.C., Gilbert, H.B., Nill, S.T., Russell, P.T., Weaver, K.D., Webster, R.J., 2011. A bimanual teleoperated system for endonasal skull base surgery, in: 2011 IEEE/RSJ international conference on intelligent robots and systems, IEEE. pp. 2517–2523.

- [5] Burgner-Kahrs, J., Rucker, D.C., Choset, H., 2015. Continuum robots for medical applications: A survey. *IEEE Transactions on Robotics* 31, 1261–1280.
- [6] Chikhaoui, M.T., Rabenorosoa, K., Andreff, N., 2016. Kinematics and performance analysis of a novel concentric tube robotic structure with embedded soft micro-actuation. *mechanism and Machine Theory* 104, 234–254.
- [7] Chirikjian, G.S., Burdick, J.W., 1994. A modal approach to hyper-redundant manipulator kinematics. *IEEE Transactions on Robotics and Automation* 10, 343–354.
- [8] Dupont, P., Gosline, A., Vasilyev, N., Lock, J., Butler, E., Folk, C., Cohen, A., Chen, R., Schmitz, G., Ren, H., et al., 2012. Concentric tube robots for minimally invasive surgery, in: *hamlyn symposium on medical robotics*, p. 8.
- [9] Dupont, P.E., Lock, J., Butler, E., 2009. Torsional kinematic model for concentric tube robots, in: *2009 IEEE International Conference on Robotics and Automation*, IEEE. pp. 3851–3858.
- [10] Dupont, P.E., Lock, J., Itkowitz, B., 2010. Real-time position control of concentric tube robots, in: *2010 IEEE International Conference on Robotics and Automation*, IEEE. pp. 562–568.
- [11] Fagogenis, G., Bergeles, C., Dupont, P.E., 2016. Adaptive non-parametric kinematic modeling of concentric tube robots, in: *2016 IEEE/RSJ International Conference on Intelligent Robots and Systems (IROS)*, IEEE. pp. 4324–4329.
- [12] Garriga-Casanovas, A., Rodriguez y Baena, F., 2018. Complete follow-the-leader kinematics using concentric tube robots. *The International Journal of Robotics Research* 37, 197–222.
- [13] George Thuruthel, T., Falotico, E., Manti, M., Pratesi, A., Cianchetti, M., Laschi, C., 2017. Learning closed loop kinematic controllers for continuum manipulators in unstructured environments. *Soft robotics* 4, 285–296.
- [14] Gilbert, H.B., Neimat, J., Webster, R.J., 2015. Concentric tube robots as steerable needles: Achieving follow-the-leader deployment. *IEEE Transactions on Robotics* 31, 246–258.
- [15] Gilbert, H.B., Rucker, D.C., Webster III, R.J., 2016. Concentric tube robots: The state of the art and future directions, in: *Robotics Research*. Springer, pp. 253–269.
- [16] Giorelli, M., Renda, F., Calisti, M., Arienti, A., Ferri, G., Laschi, C., 2015. Neural network and jacobian method for solving the inverse statics of a cable-driven soft arm with nonconstant curvature. *IEEE Transactions on Robotics* 31, 823–834.
- [17] Grassmann, R., Modes, V., Burgner-Kahrs, J., 2018. Learning the forward and inverse kinematics of a 6-dof concentric tube continuum robot in se (3), in: *2018 IEEE/RSJ International Conference on Intelligent Robots and Systems (IROS)*, IEEE. pp. 5125–5132.
- [18] Grazioso, S., Di Gironimo, G., Siciliano, B., 2018. From differential geometry of curves to helical kinematics of continuum robots using exponential mapping, in: *International Symposium on Advances in Robot Kinematics*, Springer. pp. 319–326.
- [19] Ha, J., Fagogenis, G., Dupont, P.E., 2018. Modeling tube clearance and bounding the effect of friction in concentric tube robot kinematics. *IEEE Transactions on Robotics* 35, 353–370.
- [20] Kim, C., Ryu, S.C., Dupont, P.E., 2015. Real-time adaptive kinematic model estimation of concentric tube robots, in: *2015 IEEE/RSJ International Conference on Intelligent Robots and Systems (IROS)*, IEEE. pp. 3214–3219.
- [21] Kuntz, A., Sethi, A., Webster, R.J., Alterovitz, R., 2020. Learning the complete shape of concentric tube robots. *IEEE Transactions on Medical Robotics and Bionics* .
- [22] Liu, S.T., Chen, C., 2017. Framework of modelling concentric tube robot and comparison on computational efficiency. *Meccanica* 52, 2201–2217.
- [23] Lock, J., Dupont, P.E., 2011. Friction modeling in concentric tube robots, in: *2011 IEEE International Conference on Robotics and Automation*, IEEE. pp. 1139–1146.
- [24] Mahl, T., Hildebrandt, A., Sawodny, O., 2014. A variable curvature continuum kinematics for kinematic control of the bionic handling assistant. *IEEE transactions on robotics* 30, 935–949.
- [25] Miele, A., Aggarwal, A., Tietze, J., 1974. Solution of two-point boundary-value problems with jacobian matrix characterized by large positive eigenvalues. *Journal of Computational Physics* 15, 117–133.
- [26] Murray, R.M., 2017. *A mathematical introduction to robotic manipulation*. CRC press.
- [27] Ni, W., Cheng, D., Hu, X., 2008. Minimum dwell time for stability and stabilization of switched linear systems, in: *2008 7th World Congress on Intelligent Control and Automation*, IEEE. pp. 4109–4115.
- [28] Peyron, Q., Rabenorosoa, K., Andreff, N., Renaud, P., 2019. A numerical framework for the stability and cardinality analysis of concentric tube robots: Introduction and application to the follow-the-leader deployment. *Mechanism and Machine Theory* 132, 176–192.
- [29] Renda, F., Boyer, F., Dias, J., Seneviratne, L., 2018. Discrete cosserat approach for multisection soft manipulator dynamics. *IEEE Transactions on Robotics* 34, 1518–1533.
- [30] Renda, F., Cianchetti, M., Abidi, H., Dias, J., Seneviratne, L., 2017. Screw-based modeling of soft manipulators with tendon and fluidic actuation. *Journal of Mechanisms and Robotics* 9.
- [31] Renda, F., Seneviratne, L., 2018. A geometric and unified approach for modeling soft-rigid multi-body systems with lumped and distributed degrees of freedom, in: *2018 IEEE International Conference on Robotics and Automation (ICRA)*, IEEE. pp. 1567–1574.
- [32] Roesthuis, R.J., Misra, S., 2016. Steering of multisegment continuum manipulators using rigid-link modeling and fbg-based shape sensing. *IEEE transactions on robotics* 32, 372–382.
- [33] Rone, W.S., Ben-Tzvi, P., 2014. Mechanics modeling of multisegment rod-driven continuum robots. *Journal of Mechanisms and Robotics* 6, 041006.
- [34] Rucker, D.C., Jones, B.A., Webster III, R.J., 2010a. A geometrically exact model for externally loaded concentric-tube continuum robots. *IEEE Transactions on Robotics* 26, 769–780.
- [35] Rucker, D.C., Webster, R.J., 2011. Computing jacobians and compliance matrices for externally loaded continuum robots, in: *2011 IEEE International Conference on Robotics and Automation*, IEEE. pp. 945–950.
- [36] Rucker, D.C., Webster III, R.J., 2011. Statics and dynamics of continuum robots with general tendon routing and external loading. *IEEE Transactions on Robotics* 27, 1033–1044.
- [37] Rucker, D.C., Webster III, R.J., Chirikjian, G.S., Cowan, N.J., 2010b. Equilibrium conformations of concentric-tube continuum robots. *The International journal of robotics research* 29, 1263–1280.
- [38] Sears, P., Dupont, P., 2006. A steerable needle technology using curved concentric tubes, in: *2006 IEEE/RSJ international conference on intelligent robots and systems*, IEEE. pp. 2850–2856.
- [39] Sloss, J., 1970. The bending of space curves into piecewise helical curves. *Pacific Journal of Mathematics* 32, 231–239.
- [40] Vasilyev, N.V., Gosline, A.H., Veeramani, A., Wu, M.T., Schmitz, G.P., Chen, R.T., Arabagi, V., Del Nido, P.J., Dupont, P.E., 2015. Tissue removal inside the beating heart using a robotically delivered metal mems tool. *The International Journal of Robotics Research* 34, 236–247.
- [41] Webster, R.J., Swensen, J.P., Romano, J.M., Cowan, N.J., 2009. Closed-form differential kinematics for concentric-tube continuum robots with application to visual servoing, in: *Experimental Robotics*, Springer. pp. 485–494.
- [42] Webster III, R.J., Jones, B.A., 2010. Design and kinematic modeling of constant curvature continuum robots: A review. *The International Journal of Robotics Research* 29, 1661–1683.
- [43] Webster III, R.J., Romano, J.M., Cowan, N.J., 2008. Mechanics of precurved-tube continuum robots. *IEEE Transactions on Robotics* 25, 67–78.
- [44] Xu, R., Asadian, A., Naidu, A.S., Patel, R.V., 2013. Position control of concentric-tube continuum robots using a modified Jacobian-based approach, in: *Proceedings - IEEE International Conference on Robotics and Automation*. doi:10.1109/ICRA.2013.6631413.
- [45] Xu, R., Patel, R., 2012. A fast torsionally compliant kinematic model of concentric-tube robots, in: *2012 Annual International Conference*

of the IEEE Engineering in Medicine and Biology Society, IEEE. pp. 904–907.

- [46] Xu, R., Yurkewich, A., Patel, R.V., 2016. Curvature, torsion, and force sensing in continuum robots using helically wrapped fbg sensors. *IEEE Robotics and Automation Letters* 1, 1052–1059.
- [47] Yip, M.C., Camarillo, D.B., 2014. Model-less feedback control of continuum manipulators in constrained environments. *IEEE Transactions on Robotics* 30, 880–889.



Mahdi Pourafzal received the B.Sc. degree from Shahed University, Tehran, Iran, in 2010, and the M.Sc. degree from K. N. Toosi University of Technology, Tehran, Iran, in 2013, both in electrical engineering. He is currently pursuing the Ph.D. degree in electrical engineering at Amirkabir University of Technology, Tehran, Iran. His research interests include medical robotics, continuum robotics and control of nonlinear systems.



Heidar A. Talebi received the B.Sc. degree in electrical engineering from Ferdowsi University, Mashhad, Iran, in 1988, the M.Sc. degree in electrical engineering from Tarbiat Modarres University, Tehran, Iran, in 1991, and the Ph.D. degree in electrical engineering from Concordia University, Montreal, QC, Canada, in 1997. He was a Postdoctoral Fellow and a Research Fellow with Concordia University and the University of Western Ontario. In 1999, he joined the Amirkabir University of Technology, Tehran, where he is currently a Professor and the Chair of the Department of Electrical Engineering. His research interests include control, robotics, medical robotics, fault diagnosis and recovery, intelligent systems, adaptive control, nonlinear control, and real-time systems.



Kanty Rabenorosoa received the M.S. degree in electrical engineering from Institut National des Sciences Appliquées Strasbourg, Strasbourg, France, in 2007, and the Ph.D. degree in automatic control from the University of Franche-Comté, Besançon, France, in 2010. He was a Post-Doctoral Fellow at Laboratoire d'Informatique, de Robotique et de Micro-électronique de Montpellier, University of Montpellier, France, from 2011 to 2012. He is currently an Associate Professor with the AS2M Department, FEMTO-ST Institute, Besançon. His research interests includes mechatronics, smart actuator, soft and continuum micro-robotics for medical applications within the Micro-NanoRobotics team.